EJNMMI Research

ORIGINAL RESEARCH

Open Access

Evaluation of damage discrimination in dopaminergic neurons using dopamine transporter PET tracer [^{18}F]FECNT-d$_4$

Jie Tang[1], Congjin Liu[2], Chunyi Liu[1], Qianyue Hu[1], Yi Fang[1] and Zhengping Chen[1*]

Abstract

Background Parkinson's disease (PD) is a prevalent neurodegenerative disorder worldwide, diagnosed based on classic symptoms like motor dysfunction and cognitive impairments. With the development of various radioactive ligands, positron emission tomography (PET) imaging combined with specific radiolabelling probes has proven to be effective in aiding clinical PD diagnosis. Among these probes, 2β-Carbomethoxy-3β-(4-chlorophenyl)-8-(2-[^{18}F]-fluoroethyl) nortropane ([^{18}F]FECNT) has been utilized as a PET tracer to image dopamine transporter (DAT) integrity in striatal presynaptic dopaminergic terminals. However, the presence of brain-penetrant radioactive metabolites produced by [^{18}F]FECNT may impact the accuracy of PET imaging. In previous research, we developed 2β-Carbomethoxy-3β-(4-chlorophenyl)-8-(2-[^{18}F]-fluoroethyl-1,1,2,2-d4) nortropane ([^{18}F]FECNT-d$_4$), a deuterated derivative with enhanced stability in plasma and the striatum, along with a slower washout rate. In this study, we further investigated the potential of [^{18}F]FECNT-d$_4$ to detect dopaminergic neuron degeneration in Parkinson's disease. This involved PET imaging in unilaterally-lesioned PD model rats and in vitro autoradiography conducted on postmortem brain sections.

Results PET images revealed reduced specific uptake in the ipsilateral striatum of rats stereotactically injected with 6-hydroxydopamine hydrochloride (6-OHDA). Compared to the sham group, the ratio of standardized uptake value (SUV) in the ipsilateral to contralateral striatum decreased by 13%, 23%, and 63% in the mild, moderate, and severe lesioned groups, respectively. Dopaminergic denervation observed in PET imaging was further supported by behavioral assessments, immunostaining, and monoamine concentration tests. Moreover, the microPET results exhibited positive correlations with these measurements, except for the apomorphine-induced rotational behavior test, which showed a negative correlation. Additionally, [^{18}F]FECNT-d$_4$ uptake was approximately 40% lower in the postmortem striatal sections of a PD patient compared to a healthy subject. Furthermore, estimated human dosimetry (effective dose equivalent: 5.06 E-03 mSv/MBq), extrapolated from rat biodistribution data, remained below the current Food and Drug Administration limit for radiation exposure.

Conclusion Our findings demonstrate that [^{18}F]FECNT-d$_4$ accurately estimates levels of dopaminergic neuron degeneration in the 6-OHDA-induced PD rat model and effectively distinguishes between PD patients and healthy

*Correspondence:
Zhengping Chen
chenzhengping@jsinm.org

Full list of author information is available at the end of the article

individuals. This highly sensitive and safe PET probe holds promising potential for clinical application in the diagnosis and monitoring of Parkinson's disease.

Keywords Parkinson's Disease, DAT, microPET, [^{18}F]FECNT-d$_4$, Rat model

Backgound

Parkinson's disease (PD) stands as one of the most prevalent neurological disorders, experiencing a notable rise in prevalence [1, 2]. Currently, PD diagnosis primarily relies on classic motor symptoms including akinesia, rigidity, bradykinesia, resting tremors, and postural instability, alongside mood, emotion, and cognition abnormalities. However, as these clinical symptoms may overlap with other neuropsychiatric syndromes, this diagnostic approach may not be comprehensive enough, especially in premotor and early motor stages [3, 4]. Additionally, typical symptoms often manifest only in the advanced or late stages of PD. To achieve a definitive diagnosis of PD in the early stages and differentiate it from other syndromes, neuroimaging techniques have been developed to objectively characterize neurobiochemical alterations in the living human brain [5, 6]. These non-invasive techniques offer rapid imaging at the cellular and molecular levels, providing visible insights into neurobiochemical dysfunctions. Among these techniques, positron emission tomography (PET) is particularly adept at quantifying physiological, biochemical, and pathological processes in neurodegenerative diseases [7, 8]. With the well-documented dopaminergic degeneration in PD, PET imaging targeted at various biomarkers in the dopaminergic system offers valuable insights into the underlying pathophysiological and mechanical abnormalities [9, 10]. For instance, L-3,4-dihydroxy-6-^{18}Ffluoro-phenylalanine ([^{18}F]F-DOPA), a radiotracer to assess dopamine synthesis and metabolism through aromatic L-amino acid decarboxylase (AADC), is the first imaging agent approved in the EU and the US in 2019 for diagnosing PD by evaluating dopaminergic function in vivo [11]. However, it has been showed that AADC activity is upregulated in early PD, possibly due to compensatory changes in presynaptic dopaminergic nerve terminals, while DAT density, which is less affected, shows downregulation. Additionally, from another pathological perspective, the dopamine transporter (DAT), another presynaptic biomarker, has been identified as important, valuble and complementary [11, 12]. DAT plays a significant role in detecting the loss of nigrostriatal dopaminergic nerve endings and has has gained traction as a valuable tool in clinical and preclinical studies [13, 14].

The dopamine transporter, a protein expressed in presynaptic dopaminergic neurons, is responsible for regulating the spatial release and reuptake of dopamine (DA) by pumping released DA from the synaptic cleft back into the presynaptic neuron [15, 16]. DAT expression level has a close relationship with striatal dopaminergic innervation and nigral cell loss [17]. Dysregulation of DAT can disrupt central dopamine homeostasis, which is a pathological characteristic of PD [18]. Studies have shown that DAT serves as a suitable biomarker for dopamine neuron integrity, making it a target for in vivo imaging probes. DAT imaging is thus a valuable tool for visualizing structural and functional degeneration, aiding in PD diagnosis, monitoring of disease progression, and evaluation of therapy efficiency [19, 20]. Over recent decades, several radioligands based on tropane derivatives, including [^{11}C] CFT, [^{11}C]WIN-35,428, [^{18}F]FE-PE2I, [^{18}F]LBT-999, [^{18}F] FP-CIT, and 2β-Carbomethoxy-3β- (4-chlorophenyl)-8-(2-[^{18}F]-fluoroethyl) nor tropane ([^{18}F]FECNT), have been developed to selectively visualize the degeneration of dopaminergic neurons targeting DAT using PET imaging [21–25]. These radioligands provide essential neurological information for PD diagnosis and treatment [6, 26].

Among these tracers, [^{18}F]FECNT is one of the potential probes for distinguishing striatal dopamine denervation in Parkinson's patients, boasting high selectivity and specific affinity for DAT (ki=1.5 nM) [27, 28]. However, it has some shortcomings, such as susceptibility to dealkylation by cytochrome P450 enzymes, resulting in the formation of radioactive metabolites like [^{18}F]fluoroacetaldehyde, [^{18}F]fluoroacetatic acid, and [^{18}F]fluoroethanol. These brain-penetrant metabolites produced by [^{18}F] FECNT can generate significant radioactive background signals, leading to confounding quantitative measurements of PET imaging [29]. Thus, substituting hydrogen with deuterium in metabolizable positions of candidate pharmaceuticals is a common strategy to enhance metabolic stability, including for radiotracers [30–32]. Deuterated versions of radioligands, such as [^{18}F]9-O-hexadeutero-3-fluoropropoxyl-(+)-dihydrotetrabenazine, [^{18}F]fluoro-[1,2-2H$_4$] choline, and [^{11}C]L-deprenyl-D$_2$, have been developed to modify in vivo properties of radiopharmaceuticals [33–36]. These deuterated versions exhibit improved pharmacokinetic parameters compared to their non-deuterated counterparts.

In our previous work, we introduced a deuterated [^{18}F]FECNT derivative named 2β-Carbomethoxy-3β-(4-chlorophenyl)-8-(2-[^{18}F]-fluoroethyl-1,1,2,2-d$_4$) nortropane ([^{18}F]FECNT-d$_4$), which exhibited improved in vivo metabolic stability in both the brain and plasma compared to the parent tracer [^{18}F]FECNT [37]. Building on this, our current study explores the potential application of [^{18}F]FECNT-d$_4$ in visualizing PD models. We

first verified the capacity of this deuterium-substituted radiotracer to evaluate escalating degrees of dopamine neuron loss in a rat model of Parkinson's disease induced by 6-hydroxydopamine hydrochloride (6-OHDA). By employing unilateral PD model rats treated with three different doses of 6-OHDA, we aimed to replicate the pathological characteristics observed in PD patients at various stages of the disease progression. These model rats allowed for detailed investigations at the cellular and molecular levels to elucidate the mechanisms underlying PD development. MicroPET imaging was used to evaluate the effectiveness of [^{18}F]FECNT-d$_4$ in detecting the different stages of dopaminergic neural dysfunction. Additionally, the imaging data were corroborated by behavioral, biochemical, and immunohistochemical (IHC) analyses. Furthermore, the radioactive uptake of [^{18}F]FECNT-d$_4$ and its variations under homeostatic and disease conditions were examined using in vitro autoradiography in postmortem human brain sections, providing additional evidence supporting its potential for clinical application. Radiation dosimetry based on biodistribution in rats, was estimated to predict radiological safety in human subjects. Our findings indicate that [^{18}F]FECNT-d$_4$ is a potential PET tracer targeting DAT, offering potential benefits for early and objective diagnosis, progression grading, classification, and treatment monitoring for PD. Our investigation provides support for future clinical exploration of this novel deuterated radioligand.

Methods

Experimental design

To evaluate the potential of [^{18}F]FECNT-d$_4$ in detecting various degrees of dopaminergic neuron degeneration, we utilized unilateral PD model rats treated with three doses of 6-OHDA. After a one-week acclimation period, rats were randomly assigned to sham, mild-lesioned (6 μg 6-OHDA), moderate-lesioned (18 μg 6-OHDA), and severe-lesioned (12 μg 6-OHDA) groups. We initially planned for a group size of 6 rats in the sham group and 10 per PD model group. During surgical procedures, one moderate-lesioned-group rat became moribund but survived. To maintain planned group parity, we added another animal to this group. Unfortunately, one mildly lesioned rat died one week after surgery. Consequently, the final group sizes were: sham control (n=6), mild-lesioned (n=9), moderate-lesioned (n=11), and severe-lesioned group (n=10). Following standard surgical procedures, a 4-week post-surgery period ensued, after which microPET imaging was utilized to assess dopaminergic neuron integrity. Subsequently, behavioral tests, including the open field test, cylinder test, and apomorphine (APO)-induced rotational behavior test were conducted over the subsequent three days following the PET scans. Finally, the rats were euthanized, and their brains were collected for immunochemical and biochemical analyses. Correlations between PET results and behavioral, immunochemical and biochemical tests were analyzed. Additionally, in vitro autoradiography on postmortem human brain sections was conducted to explore potential clinical applications. Radiation dosimetry extrapolation to humans was estimated to predict radiological safety in human subjects. All animal experiments were approved by the Animal Care and Use Committee of the Jiangsu Institute of Nuclear Medicine and conducted in compliance with institutional guidelines (Approval number: JSINM-2023-061). Postmortem human brain tissues from control and PD patient subjects were obtained from the Chinese Brain Bank Center, with experiments approved by the Ethics, Science and Technology Committee of Central South University (Committee reference number: 2022-scuec-039). The use of human postmortem brain tissues was also approved by the ethics committee of our institute (Approved number: YLK-202329), and all procedures were in accordance with ethical standards. The study was carried out in compliance with the ARRIVE guidelines, and all methods adhered to relevant guidelines and regulations.

Radiopharmaceutical

The precursor 2β-Carbomethoxy-3β-(4-Chlorophenyl)-8-(2-((methylsulfonyl)-oxy)ethyl-1,1,2,2-d$_4$)-nortropane (MsOECNT-d$_4$), was synthesized in our lab according to the previously reported method [35]. The radiosynthesis of [^{18}F]FECNT-d$_4$ was carried out following literature protocols as illustrated in Fig. 1. The purified radiochemical had a purity of >99.9%, and the molar activities>55 GBq/μmol.

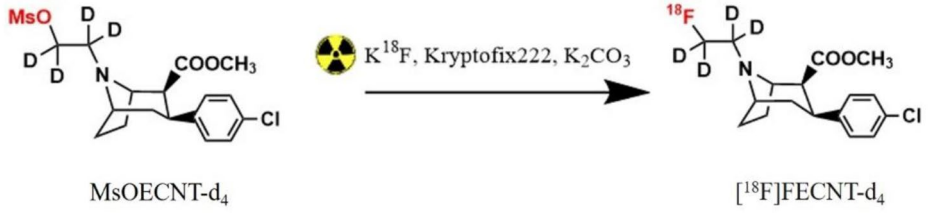

Fig. 1 Radiosynthesis of [^{18}F]FECNT-d$_4$ from precursor MsOECNT-d$_4$

Surgical procedures

The neurotoxin 6-OHDA was dissolved in saline containing 0.2% L-ascorbic acid and prepared before use according to published studies [38]. Rats were anesthetized using 2.5% isoflurane and stereotactically injected with 6-OHDA solution into the left corpus striatum at doses of 0, 6 μg, 12 μg, or 18 μg, respectively, at coordinates: AP:1.0 mm, ML: -3.0 mm, DV: 4.8 mm. The injection pace was 0.5 μL/min, and the needle was left for an additional five minutes before being slowly retracted. The stereotaxic lesion surgery was performed on two successive days.

MicroPET imaging scan and quantitative analysis

The study conducted microPET scans on model rats using [^{18}F]FECNT-d_4 on the 28th day post-surgery. A stable period of 15–35 min was selected for static scanning after intravenous injection of the radiotracer. Each rat was under isoflurane anesthesia (2.5% in oxygen gas) during the phase of 10–35 min post-injection. Imaging data were reconstructed using filtered back projection mode, and ASIPro VM software was employed for analysis. Region of interest (ROI) of the striatum (ST) and cerebellum (CB) were manually outlined according to previous literature [37, 39]. The specific uptake of [^{18}F]FECNT-d_4 was quantified as a standardized uptake value ratio (SUVr), calculated using a formula:

$$\mathrm{SUVr} = \frac{SUV(ST) - SUV(CB)}{SUV(CB)}$$

Behavioral test

Open field test

Following the PET imaging test, behavioral assessments were conducted on the animals over the subsequent three days. The open field test (OFT) and APO-induced rotation test were employed. The OFT, a classical behavioral examination, measures spontaneous locomotor activity in a drug-free state. Conducted over 5 min, the test utilized a plexiglass square arena equipped with an auto-behavior-measuring device. Parameters such as rearing number, mobility time, and total movement distance were recorded and analyzed. The experiment was carried out in a quiet and dim atmosphere. Each rat underwent testing in triplicate, and the apparatus was cleaned with 75% alcohol before each test to mitigate the influence of odors.

APO-induced unilateral rotational test

Dopamine agonists can increase asymmetric rotational behavior, serving as a characteristic indicator of damage severity in the nigrostriatal pathway. The APO-induced unilateral rotational test is commonly utilized to estimate lesion-induced dyskinesia. In this study, a dose of 0.5 mg/kg APO was administered intraperitoneally to rats, and the test duration was 30 min. The numbers of ipsilateral and contralateral turns were recorded with a mechanical rotometer device, and the rotation number was calculated as contralateral turns minus ipsilateral turns. To mitigate the effects of agonists, the APO-induced rotational test was conducted after the OFT test.

Immunochemistry

After completing all of the behavioral experiments, experimental animals were randomly divided for further immunochemical and biological analysis. For the immunochemical test, animals comprised sham control (n=3), mild-lesioned (n=4), moderate-lesioned (n=5), and severe-lesioned (n=5) groups. Rats were deeply anesthetized and perfused with approximately 200 mL of 0.01 M phosphate-buffered saline (PBS) followed by about 200 mL of 4% paraformaldehyde. The brain was then promptly removed and immersed in 4% paraformaldehyde overnight. The brain tissue was gradually dehydrated in sucrose solutions of increasing concentrations (10%, 20%, and 30%) before being embedded in optimal cutting temperature (O.C.T.) medium and stored at −80 ℃. Before use, the tissues of the ST and substantia nigra (SN) were sliced into 20 μm thick coronal sections using a microtome (Thermo, Germany). The corresponding sections were washed with PBS, blocked with bovine serum albumin (Sigma-Aldrich), and then incubated overnight at 4 ℃ with mouse anti-tyrosine hydroxylase (TH antibody, 1:500, Sigma-Aldrich, T2928). Subsequently, sections were incubated with the corresponding secondary antibody (GK600705, Gene Tech, China) and stained with 3,3'-diaminobenzidine tetrahydrochloride (DAB, GK347011, Gene Tech, China). Bilateral ST or SN sections were photographed using a conventional microscope (Olympus, X51, Japan) and digitized with Image Pro-plus software. The integral optical density (IOD) of TH-positive striatal fiber density and the number of TH-positive cells in each hemisphere (ipsilateral striatum, I-ST; contralateral striatum, C-ST; ipsilateral substantia nigra, I-SN; contralateral substantia nigra, C-SN) were quantified. Changes in the number of TH-labeled neurons were expressed as the ratio of IOD (I-ST to C-ST) or the ratio of the number of TH-positive cells (I-SN to C-SN).

Determination of levels of DA and DA metabolites

For the biological test, 3 rats in the sham group, 5 in the mild-lesioned group, 6 in the moderate-lesioned group, and 5 in the severe-lesioned group were selected. After decapitation under anesthesia overdose, the striatum of intact and lesioned sides was promptly dissected on ice and stored at − 80 ℃ until biochemical analysis. Tissue

samples were diluted and homogenized in 0.2 M perchloric acid. Following centrifugation, the supernatant was injected into high-performance liquid chromatography (HPLC) equipped with a Waters 2465 HPLC separation module and electrochemical detection (ECD) [39]. The levels of DA and its main metabolites (3,4-dihydroxyphenylacetic acid, DOPAC; and homovanillic acid, HVA) were determined using a Kinetex® C18 column with a mobile phase containing 10 mM citric acid, 0.1 mM Ethylenediaminetetraacetic Acid (EDTA), 2.0 mM 1-octanesulfonic acid, 70 mM potassium dihydrogen phosphate, and 10% methanol. The flow rate was maintained at 0.5 mL/min, and the sample temperature was kept at 4 ℃.

Autoradiography of [^{18}F]FECNT-d_4 in postmortem human brain

To evaluate the clinical applicability of [^{18}F]FECNT-d_4 in identifying pathological degeneration of dopaminergic neurons, quantitative autoradiography (ARG) was conducted on postmortem human brain sections. A calibration curve of signal intensity was generated by spotting six known amounts of radioactivity, ranging from 1.16 to 37 KBq/mL [^{18}F]FECNT-d_4, onto a slide covered with filter paper [40]. Postmortem tissues of the corpus striatum of a PD patient (82-year-old) and a healthy subject (86-year-old) were sliced on a cryostat microtome (Thermo, Germany) at 20 μm thick. Four sections per slide were incubated with [^{18}F]FECNT-d_4 (3.7 MBq/mL) at 4 °C for 1.5 h after preincubation with an ice-cold Tris solution (PH 7.4). Subsequently, all postmortem striatal slides were rinsed with the preincubation buffer for five intervals of five minutes each and air-dried at room temperature. Next, all slides (tissue sections and calibration curve) were placed in the same chamber and exposed to a phosphor screen imaging plate for 1 h. OptiQuant software (Perkin Elmer, USA) was utilized to analyze all images, and the extent of radioactive uptake was measured in digital light units (DLU) to describe the gross intensity in each tissue region.

Radiation dosimetry extrapolation to humans

Dosimetry analysis was conducted using Olinda/EXM software to estimate the absorbed doses in humans, facilitating the translation of [^{18}F]FECNT-d_4 from animal studies. The biodistribution data on rats at various time points (5, 15, 30, 60, and 120 min), as reported in our published paper [37], were used to extrapolate the estimated absorbed doses in humans. The %ID/g values were converted into %ID in humans based on the organ weight in a 73.7 kg male model provided by Olinda, using a specific formula as follows [41]. The extrapolated data was then input into Olinda to obtain the estimated effective doses.

$$\left(\frac{\%\mathrm{ID}}{g_{\mathrm{organ}}}\right)_{\mathrm{human}} = \left[\left(\frac{\%\mathrm{ID}}{g_{\mathrm{organ}}}\right)_{\mathrm{animal}} \times (\mathrm{kg}_{\mathrm{TB\,weight}})_{\mathrm{animal}}\right] \times \left(\frac{g_{\mathrm{organ}}}{\mathrm{kg}_{\mathrm{TB\,weight}}}\right)_{\mathrm{human}}$$

Statistical analysis

All data were presented as mean ± standard error of the mean (SEM) or mean ± standard deviation (SD), as specified in the figure legends. Statistical analyses were conducted using one-way analysis of variance (ANOVA) with multiple comparisons for PET imaging, behavioral tests, immunostaining tests, and biochemical data. Pearson correlation analysis was performed to evaluate the correlations between microPET quantitative results and data from biological, histological, and behavioral tests. Statistical significance was determined using GraphPad Prism software, and a p-value of <0.05 was considered significant.

Results

[^{18}F]FECNT-d_4 imaging in 6-OHDA-induced PD model rat brain

In this study, we assessed the potential of [^{18}F]FECNT-d_4 for PET imaging dopaminergic innervation by conducting microPET scans in PD model rats with three different damage levels of dopamine-containing nerve induced by unilateral 6-OHDA injection. The results demonstrated graded unilateral losses of DAT-specific binding in the ipsilateral striatum of rats exposed to 6-OHDA injection, with a significant reduction of radioactive accumulation (62.92%) observed between the sham group (SUVr ratio (I-ST to C-ST) = 1.00 ± 0.06) and the highest dose group (18 μg, SUVr ratio = 0.37 ± 0.20; $p<0.0001$). Both the 6 μg and 12 μg groups also exhibited visible reductions in SUVr ratios compared to the sham group, with statistical differences observed (6 μg group: SUVr ratio = 0.87 ± 0.06, 13% decline, $p=0.0043$; 12 μg group: SUVr ratio = 0.77 ± 0.14, 23% decline, $p=0.001$, respectively). Inter-group comparisons further revealed significant differences, except for the 6 μg group vs. 12 μg group. The quantitative analysis results and representative images of all experimental groups are depicted in Fig. 2.

Behavioral changes induced by stereoscopic injection of 6-OHDA

Unilateral lesions in nigrostriatal dopaminergic terminals with 6-OHDA resulted in motor function impairment, as evidenced by the OFT results. As illustrated in Fig. 3A, B, and C, a significant decline in spontaneous movement was observed between the sham group and the highest-dose group (18 μg) for all three parameters tested (movement distance: $p=0.0031$; mobility time: $p=0.0024$; rearing number: $p<0.0001$). The 12 μg 6-OHDA injection also decreased the rearing number and total walking distance ($p=0.003$ and 0.0403, respectively) compared to

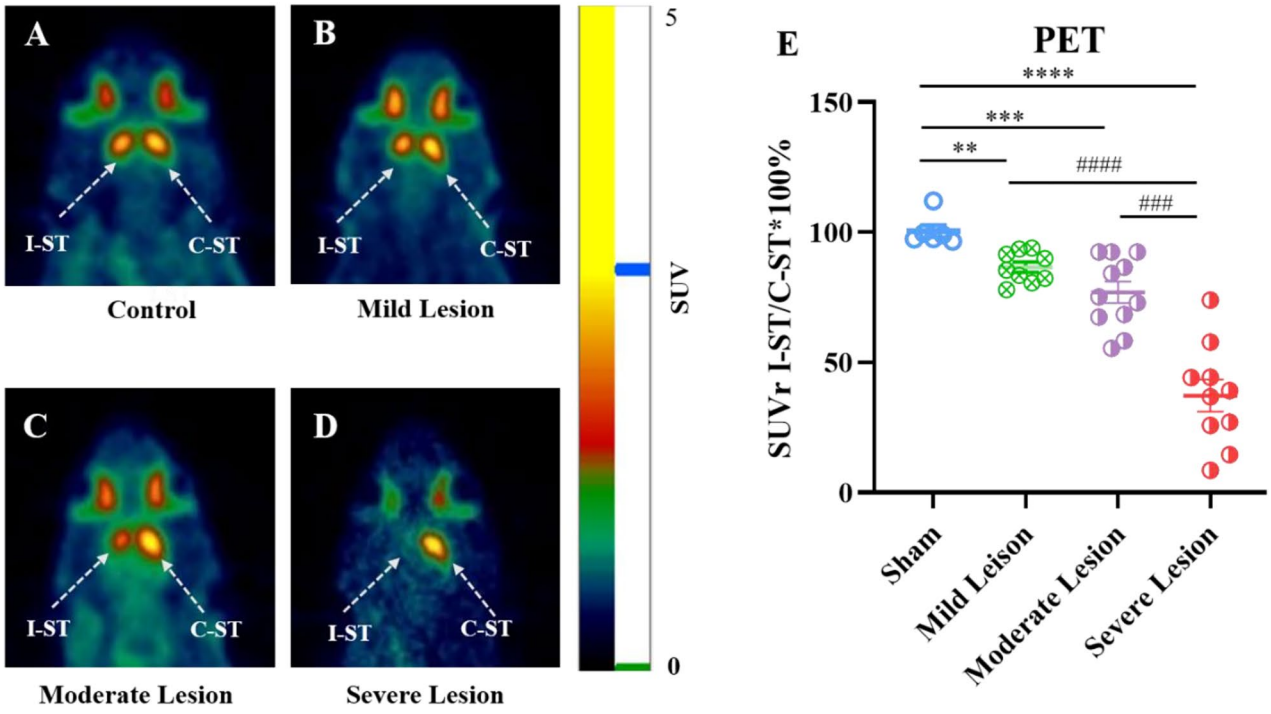

Fig. 2 MicroPET imaging results and quantitative analysis
(**A**-**D**) Representative coronal microPET images of control, mild, moderate, and severe lesion groups with [^{18}F]FECNT-d_4. (**E**) Average SUVr ratios derived from quantitative PET scan analysis. $^{**}p=0.043$, $^{***}p=0.001$, $^{****}p<0.0001$, versus sham group; $^{\#\#\#\#}p<0.0001$, $^{\#\#\#}p=0.0004$, versus severe lesion group. Data were expressed as mean ± SEM, $n=6$–11

the sham group. However, no significant difference was observed between the sham group and the mild lesion group for any of the three parameters tested.

As shown in Fig. 3D, the APO-induced rational test demonstrated that rats with severe lesions exhibited markedly high-frequency asymmetrical rotations in response to APO treatment (the efficient rotation number = 164.23 ± 94.42), while rational behavior decreased significantly in the 6 μg and 12 μg dose groups (15.42 ± 20.07 and 33.08 ± 29.46, respectively), compared to control rats, which did not exhibit biased rotational behavior (6.30 ± 4.92). The difference in rotation number between the highest dose group and other groups was significant, with *p*-values less than 0.0001. However, there was no significant difference among the sham, mild, and moderate lesion groups due to fluctuating data.

We also conducted a statistical analysis of the quantitative results from microPET scans and 6-OHDA-induced rotational studies. The analysis revealed a negative correlation between the deduction in the uptake of [^{18}F] FECNT-d_4 (% SUVr ratios I-ST to C-ST) and the number of APO-induced rotations ($r=-0.9307$, $p<0.0001$, depicted in Fig. 3E). Conversely, positive linear correlations existed between the uptake decline (% SUVr ratios I-ST to C-ST) and the outcomes of mobility time ($r=0.5919$, $p=0.0001$, depicted in Fig. 3F), movement distance ($r=0.6764$, $p<0.0001$, depicted in Fig. 3G), and rearing number ($r=0.5596$, $p=0.0004$, depicted in Fig. 3H) in the OFT.

Down-regulation of TH expression in striatum and nigra post-lesion of 6-OHDA administration

In this study, both striatal and nigral sections of 6-OHDA-treated rats exhibited a dose-dependent decrease in TH immunoreactivity, indicating a gradient reduction in dopaminergic innervation. The reduction in TH expression was quantified by digitizing the IOD of TH + striatal fiber density or TH + cell number, expressed as a percentage of the lesioned hemisphere to the intact one. Significant differences were observed in the highest and medium groups compared to the sham group for TH + striatal fiber density ($p=0.0003$ and 0.0228, respectively). The mean values were 94.48 ± 5.05% (control group), 82.19 ± 4.08% (mild group), 69.55 ± 12.94% (moderate group), and 41.84 ± 18.75% (severe group), respectively. Relative to the sham group, 18, 12, and 6 μg 6-OHDA administration decreased TH + cell number by approximately 71% ($p=0.079$), 40% ($p=0.0182$), and 18% ($p=0.0876$), respectively. Correlation analysis revealed a positive correlation between PET scans and TH expression both in the ST and SN. (TH + striatal fiber density: $r=0.9469$, $p<0.0001$; TH + cell number: $r=0.9169$,

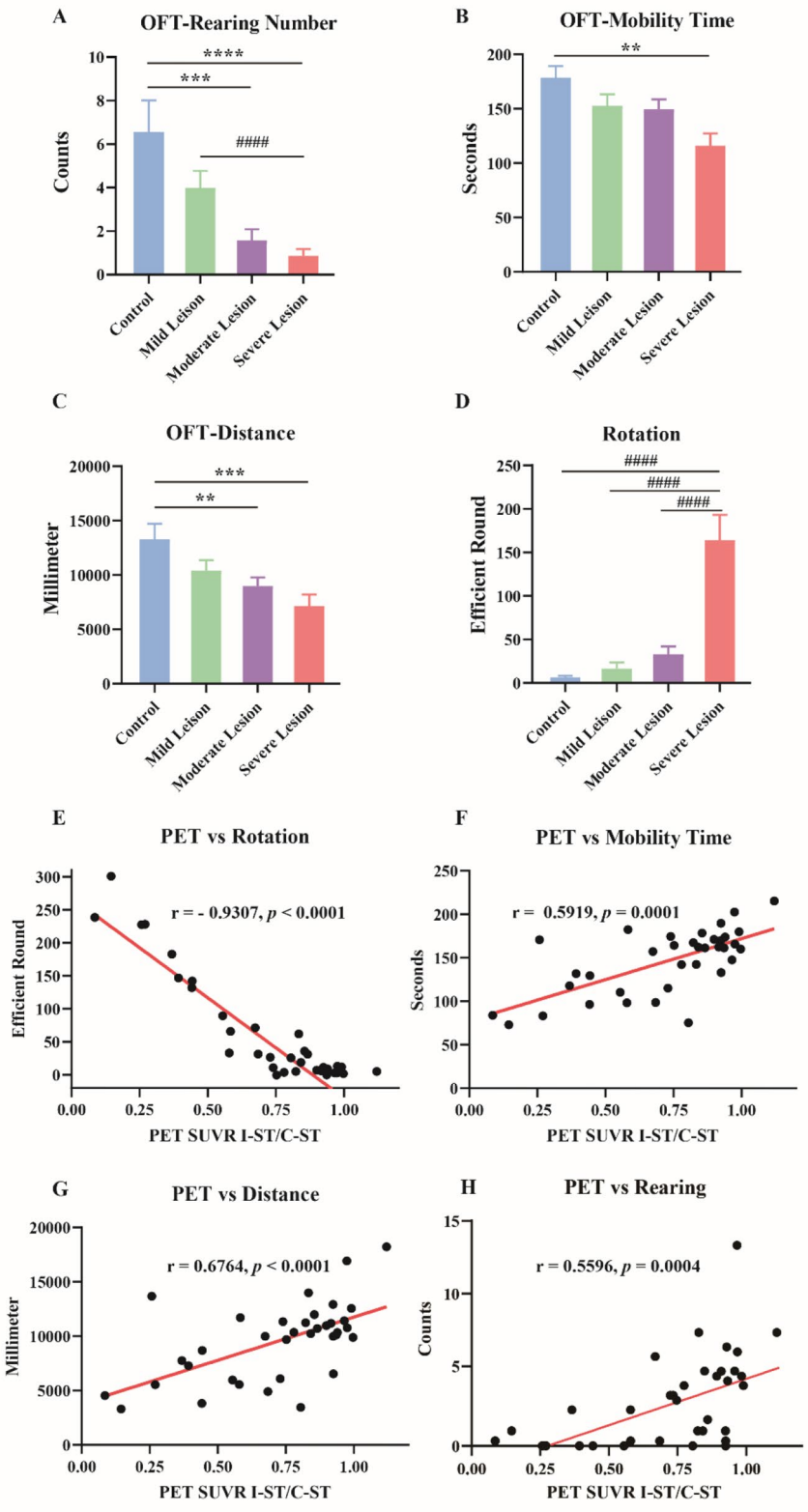

Fig. 3 Behavioral test results and correlations with PET imaging
(**A**-**C**) The parameters measured in OFT. (**D**) APO-induced rotational test results. Correlations between the behavioral test results with PET results (E-H). $^{**}p < 0.01$, $^{***}p < 0.001$, $^{****}p < 0.0001$, vs. control group; ####$p < 0.0001$, vs. lesion group

$p<0.0001$), corroborating the varying degrees of damage in the dopaminergic pathway. These findings are depicted in Fig. 4.

Biochemical evaluation of DA and DA metabolites content in striatum tissue

The result demonstrated a gradient decrease in the percentage ratio of DA content quantitation (the left to right striatum) as the dose of 6-OHDA increased (Fig. 5A). Relative to the sham group (110.41 ± 2.96%), the percentage ratio of DA content decreased approximately 73%, 27% and 26% in the severe, moderate, and mild lesion groups, respectively ($p=0.0020$, 0.0215, and 0.015, respectively). Similar trends were observed in the levels of two dopamine metabolites, DOPAC and HVA, as illustrated in Fig. 5B and C. The ratios of ipsilateral-to-contralateral DOPAC levels decreased as the 6-OHDA dose increased, with the most significant reduction observed in the severe lesion group. A similar trend was observed for HVA levels, albeit to a lesser extent. Only the highest dose group showed significant differences compared to the sham group in both DOPAC and HVA content tests. PET imaging results had a strong positive correlation with dopamine content, while correlations with DOPAC and HVA were weaker due to interindividual differences (Fig. 5D and F).

Quantitative analysis of postmortem autoradiography in human brain

The study employed in vitro autoradiography to estimate the specific binding of [^{18}F]FECNT-d_4 in postmortem striatal tissue from a PD patient and a healthy subject. A calibration curve was obtained by plotting the mean DLU value measured for each spot against the respective pre-identified radioactivity. As depicted in Fig. 6A, the digital signal intensity showed a positive correlation ($R^2=0.9834$), and the according linear equation was used to quantify the specific binding in the two groups. PD patient's striatum exhibited significantly lower specific binding as compared to healthy control brain striatum, as illustrated in Fig. 6B and C, with a decline of 39.56% ($p<0.0001$) in mean radioactive uptake (0.39 ± 0.05 Bq/mm^2 in PD vs. 0.64 ± 0.01 Bq/mm^2 in healthy control).

Radiation dosimetry extrapolation to humans

Dosimetry analysis was conducted to assess the potential clinical use of [^{18}F]FECNT-d_4 in humans. The absorbed doses to human organs were extrapolated from rat biodistribution data described in our previous study [37], using OLINDA/EXM software. Average %ID/g values were used to calculate absorbed doses, and the resulting dosimetry data is summarized in Table 1. The study showed that the liver received the highest radiation dose from [^{18}F]FECNT-d_4 (8.73 E-03 mSv/MBq), followed by the pancreas (7.24 E-03 mSv/MBq), kidneys (6.72 E-03 mSv/MBq), lungs (6.05 E-03 mSv/MBq), and spleen (6.59 E-03 mSv/MBq). It should be noted that the effective dose equivalent (5.06 E-03 mSv/MBq) was well below the Food and Drug Administration limit for the radiation burden (5 REM, amounting to 50 mSv) [42], indicating a low risk of radiotoxicity. These estimated human dosimetry data can serve to predict potential radiotoxicity before clinical trials, although further studies in humans are necessary to validate this extrapolation.

Discussion

Parkinson's disease is a progressive neurodegenerative disorder, and loss of nigrostriatal dopaminergic neurons can be detected non-invasively using PET. While [^{18}F]FDOPA is the most common tracer in PD research, reflecting nigrostriatal presynaptic function through its accumulation. Uptake of [^{18}F]FDOPA correlates with dopamine neurons only in the striatum, not the substantia nigra [43, 44]. Additionally, it suffers from high non-specific uptake in other brain regions [45]. Studies suggest that DAT-targeted PET tracers have specific uptake both in ST and SN, and might be more sensitive and accurate, particularly in early PD [5, 11, 46]. [^{18}F]FECNT, proposed as a PET imaging ligand for estimating PD-related dopamine transporter density, showed a promising correlation with postmortem biochemical and TH immunoreactivity intensity measurements [27]. However, radiometabolites of [^{18}F]FECNT were shown to penetrate the blood-brain barrier (BBB) [43], leading to non-specific brain distribution and hindering PET quantification [29]. To overcome this limitation, we strategically replaced a Carbon-Hydrogen (C-H) bond at the N-position with a carbon-deuterium (C-D) bond. The resulting deuterated analog, [^{18}F]FECNT-d_4, displayed not only comparable affinity for DAT and lipophilicity, but also exhibited enhanced in vivo stability and reduced radiometabolites formation in both brain and plasma. Additionly, [^{18}F]FECNT-d_4 achieved a similar SUV in ST to [^{18}F]N-3-Fluoropropyl-2β-carbomethoxy-3β-(4-iodophenyl) nortropane ([^{18}F]FP-CIT), a well-established DAT radioligand [47, 48], which is also known to suffer from radiometabolite issues [49]. Based on these promising findings, we aimed to investigate the potential of [^{18}F]FECNT-d_4 as a superior candidate for visualizing DAT density in clinical applications.

This study focuses on the possibility and feasibility of [^{18}F]FECNT-d_4 to discriminate different damage levels in dopaminergic neurons, specifically in the lower phases simulating the initial and middle stages of PD, with a well-established rodent model. While previous imaging investigations have been conducted on fully-lesioned and healthy rats [37], as a part of pharmacodynamical research, this study seeks to provide specific

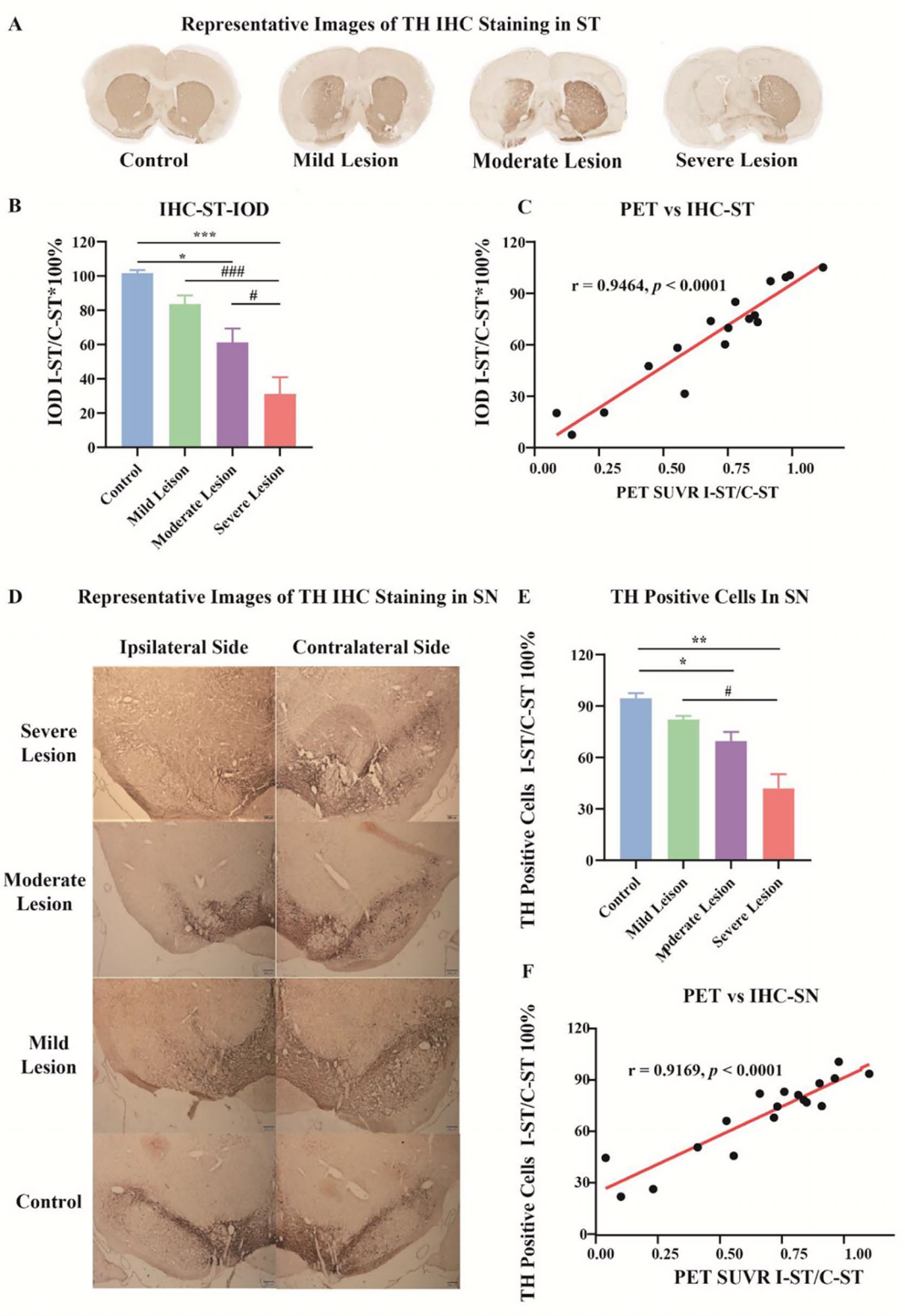

Fig. 4 Immunohistochemical Results and Quantitative Analysis

(**A**) Representative photomicrographs of TH immunostaining in the striatum. (**B**) Quantitative analysis of IOD of TH^+ striatal fiber density. (**C**) Strong positive correlation between PET results and TH-labeled striatal fiber density. (**D**) Representative photomicrographs of TH^+ cell numbers in SN tissue. (**E**) Digitization of TH^+ cell numbers in substantia nigra. (**F**) PET results correlated positively with TH^+ cell number in SN. $^{*}p < 0.05$, $^{**}p < 0.01$, $^{***}p < 0.001$, vs. group; $^{\#}p < 0.05$, $^{\#\#\#}p < 0.001$, vs. lesion group

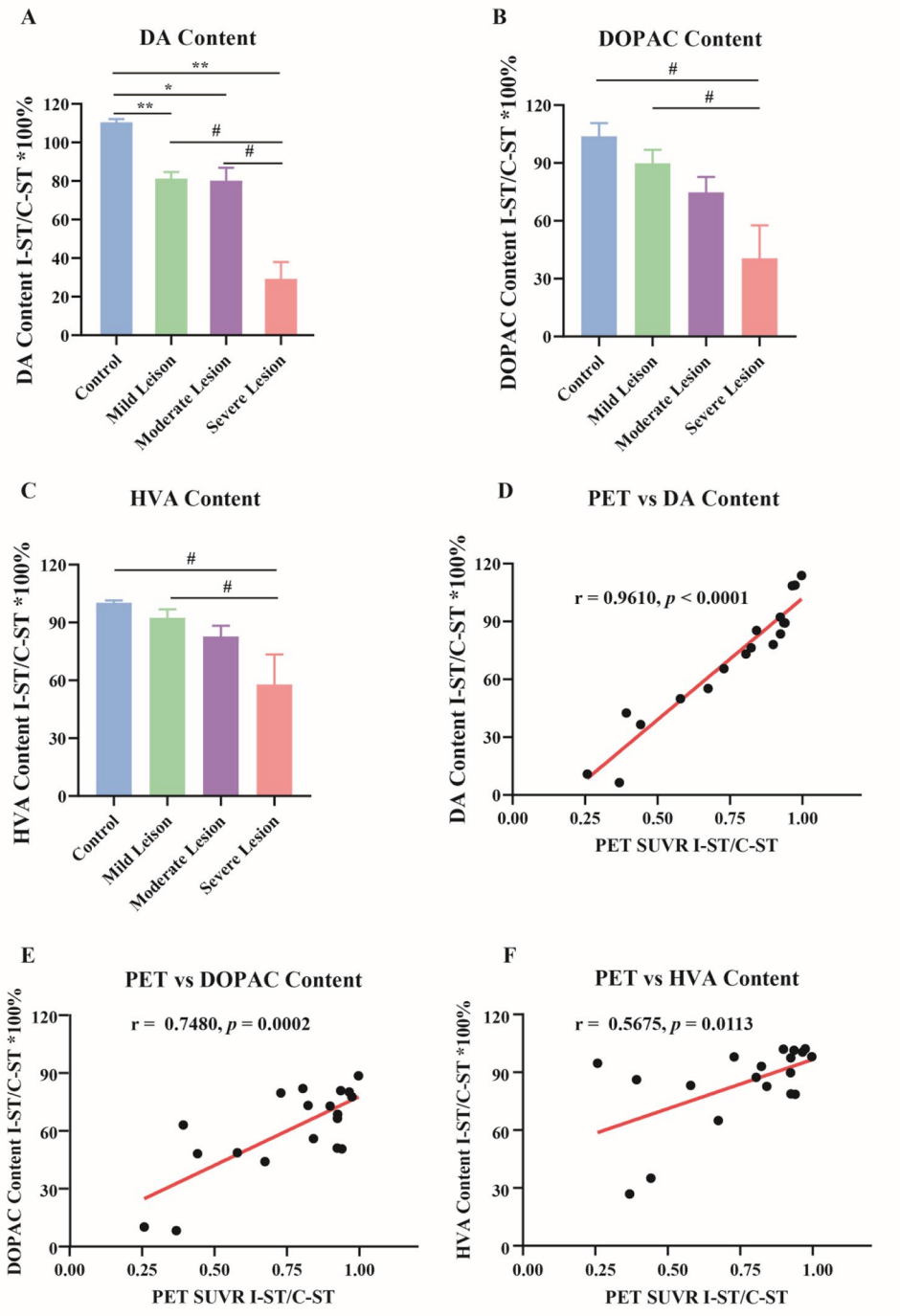

Fig. 5 Content of DA and Its metabolites in 6-OHDA-lesioned rats
(**A**-**C**) The digital diagrams show the percentage ratio of DA and its metabolites (DOPAC and HVA) content quantitation. The symbols denote *p*-value ($^{*}p < 0.05$, $^{**}p < 0.01$, versus control group; $^{\#}p < 0.05$, versus severe lesion group). (**D**) Strong positive correlation between PET results and biochemical evaluation of DA content. However, the correlation with DOPAC and HVA content was weak comparatively (**E**-**F**)

images depicting the accumulation of [^{18}F]FECNT-d$_4$ in the brains of rats with mild and moderate lesion levels. Such images can offer crucial pathological insights into PD progression and provide visual evidence supporting the clinical application of [^{18}F]FECNT-d$_4$.

MicroPET scanning with [^{18}F]FECNT-d$_4$ showed that the methodology is efficient in delineating the striatum, allowing for differentiation among the sham, mild, moderate, and severe lesion groups. The altered coupling ratio of specific uptake between the ipsilateral and contralateral striatum can distinguish between these groups.

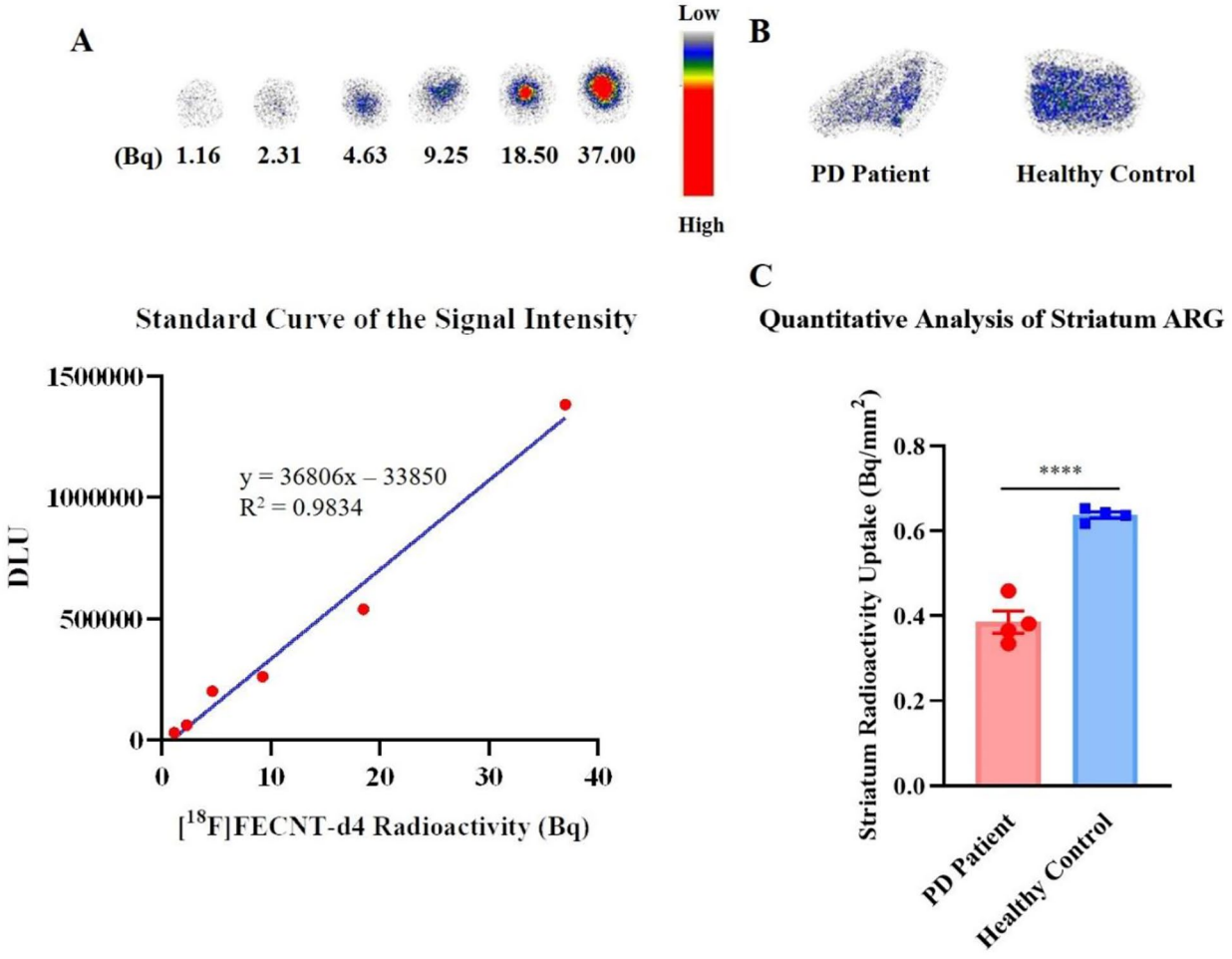

Fig. 6 Postmortem Autoradiography in Human Striatum
(**A**) Standard curve of the signal intensity at different amounts of radioactivity of [^{18}F]FECNT-d_4. (**B**) Representative in vitro autoradiography images of PD patient (82-year-old) striatum tissue and healthy subject (86-year-old) striatum tissue. (**C**) The comparative in vitro autoradiography quantitative analysis of [^{18}F]FECNT-d_4 in striatum tissue demonstrates significantly lower specific binding in the PD patient compared to the healthy human control. The results are expressed as means ± SEM of three independent measurements. $^{****}p < 0.0001$, versus healthy control

The different degrees of decline in the ratio detected by microPET were about 14% (mild), 23% (moderate), and 63% (severe) compared to the control group. These findings suggested a dose-dependent decrease in dopaminergic neuronal deficiency, which correlated with decreasing levels of DA content (mild: 26%, moderate: 27%, severe: 73%) and TH expression (mild: 18%, moderate: 40%, severe: 71%). However, TH staining was unable to differentiate between mild DA-depletion and sham group, both in terms of TH^+ neuron cell bodies in the SN and dopaminergic fiber density in the ST. These observations imply that microPET imaging with [^{18}F]FECNT-d_4 could provide valuable information about functional denervation of the dopamine system and warrants further investigation in both preclinical and clinical studies, especially in the premotor phase of Parkinson's disease.

In this study, we observed that the denervation detected by measuring dopamine content and TH expression in striatal dopaminergic neurons appeared more severe than what was revealed by microPET imaging. Several factors contribute to these discrepancies. First, administration of 6-OHDA may lead to a greater reduction in striatal dopamine levels compared to dopamine uptake sites, such as DAT [50]. Previous studies have indicated that surviving neurons may also be compromised in their ability to synthesize and metabolize dopamine following exposure to the neurotoxin. Consequently, the reduction of DA uptake, which reflects the level of dopaminergic cell death, may occur at a lower rate than the loss of DA content and TH expression levels [51]. Additionally, the effects of anesthesia which were noticed attentively by researchers, may have influenced the observed results [52, 53]. Moreover, the partial volume effect and a bias parameter in vivo related to the intrinsic properties of the scanning device should be also taken into consideration, when interpreting the imaging data. These

Table 1 Estimated radiation absorbed by adult male human

Target Organ	Total Doses (mSv/MBq)	Phantom Organ Masses (g) for the Adult Male
Adrenals	3.22 E-03	16.3
Brain	1.57 E-03	1420.0
Breasts	1.24 E-03	351.0
Gallbladder Wall	3.65 E-03	10.5
LLI wall	2.60 E-03	167.0
Small Intestine	5.41 E-03	677.0
Stomach Wall	3.92 E-03	158.0
ULI Wall	2.81 E-03	220.0
Heart Wall	4.89 E-03	316.0
Kidneys	6.72 E-03	299.0
Liver	8.73 E-03	1910.0
Lungs	6.05 E-03	1000.0
Muscle	5.33 E-03	28000.0
Ovaries	2.94 E-03	8.71
Pancreas	7.24 E-03	94.3
Red Marrow	3.71 E-03	1120.0
Osteogenic Cells	2.85 E-03	120.0
Skin	1.33 E-03	3010.0
Spleen	6.59 E-03	183.0
Testes	5.89 E-03	39.1
Thymus	2.41 E-03	20.9
Thyroid	2.13 E-03	20.7
Urinary Bladder Wall	2.47 E-03	47.6
Uterus	2.81 E-03	79.0
Total Body	3.64 E-03	73700.0
Effective Dose Equivalent (mSv/MBq)	5.06 E-03	

Dosimetry analysis was conducted using Olinda/EXM software to estimate the absorbed doses in humans, facilitating the translation of [^{18}F]FECNT-d_4 from the biodistribution data on rats. The %ID/g values were converted into %ID in humans based on the organ weight in a 73.7 kg male model provided by Olinda

factors collectively highlight the complexity of accurately assessing dopaminergic denervation and underscore the importance of integrating multiple measurement modalities for a comprehensive understanding of Parkinson's disease pathology.

The behavioral results revealed that no obvious motor-functional symptoms, such as APO-induced asymmetrical rotations and spontaneous movement, were observed in the mild group. This finding is consistent with previous research [45] and clinical postmortem investigations suggesting that physical symptoms may only manifest when striatal dopamine levels decline by more than 70% [46]. These results underscore the importance of developing effective non-invasive technologies to visualize the degeneration of dopaminergic neurons in the nigrostriatal pathway for accurate diagnosis of early PD pathophysiology.

The study further investigated the correlation between data from behavioral tests and the results of immunohistochemical tests or DA content determination. The results showed that there was no significant correlation between the parameters from the OFT and DA content in the striatum (mobility time: $r=0.4354$, $p=0.0709$; movement distance: $r=0.3559$, $p=0.1472$; rearing number: $r=0.4971$, $p=0.0358$, Fig. 7A, B, and C). However, a negative correlation was found between rotation test data and DA levels. Interestingly, PET imaging with [^{18}F]FECNT-d_4 showed a stronger correlation with behavioral tests than DA content (mobility time: $r=0.5919$, $p=0.0001$; movement distance: $r=0.6764$, $p<0.0001$; rearing number: $r=0.5596$, $p=0.004$, Fig. 3F, G, and H). Additionally, the PET results were comparable to TH positive cell number in SN (mobility time: $r=0.6735$, $p=0.0022$; movement distance: $r=0.6705$, $p=0.0023$; rearing number: $r=0.6437$, $p=0.0039$, Fig. 7D, E, and F). In the meantime, the quantitation of PET imaging also correlated well with biological and immunohistochemical results, indicating that it is a non-invasive method that can visualize dopaminergic neuronal degeneration and reflect motor functional deficits to some extent. The study suggests that PET imaging has the potential to distinguish PD patients or model rats in premotor stages from those in motor stages. However, it should be confirmed whether anesthesia (isoflurane) used in this study altered [^{18}F]FECNT-d_4 binding to DAT.

Our preclinical study in rodents estimated the efficacy, specificity, and sensitivity of [^{18}F]FECNT-d_4 to DAT. However, its selective binding in the human brain remains to be investigated for clinical applications. To approach this aim, we conducted in vitro ARG using postmortem striatal tissue from one healthy subject as well as one PD patient. The ARG results revealed that specific binding in the striatum sections from healthy subject's brains was approximately 2.5-fold higher than those from PD patient, indicating a noticeably decreased uptake in patient's brain. This finding aligns with our previous preclinical study in rats [37], suggesting that [^{18}F]FECNT-d_4 may be a feasible tool to detect dopaminergic denervation in the nigrostriatal pathway and has adequate sensitivity to diagnose Parkinson's disease in humans. However, due to the limited availability of tissue samples from PD patients across a spectrum of disease severity, we were unable to assess the efficacy of [^{18}F]FECNT-d_4 on multiple samples. Future clinical trials may provide insight into treatment protocols, disease progression tracking, and potential patient stratification.

In this study, whole-body radiation dosimetry was conducted to ensure the safety of using [^{18}F]FECNT-d_4 in human translation. The effective dose equivalent extrapolated from biodistribution data of rats was 5.06E-03 mSv/MBq, which was lower than a previous study's estimate for [^{18}F]FECNT extrapolated from primates (2.14 E-02–2.27 E-02 mSv/MBq) [54] and from studies involving

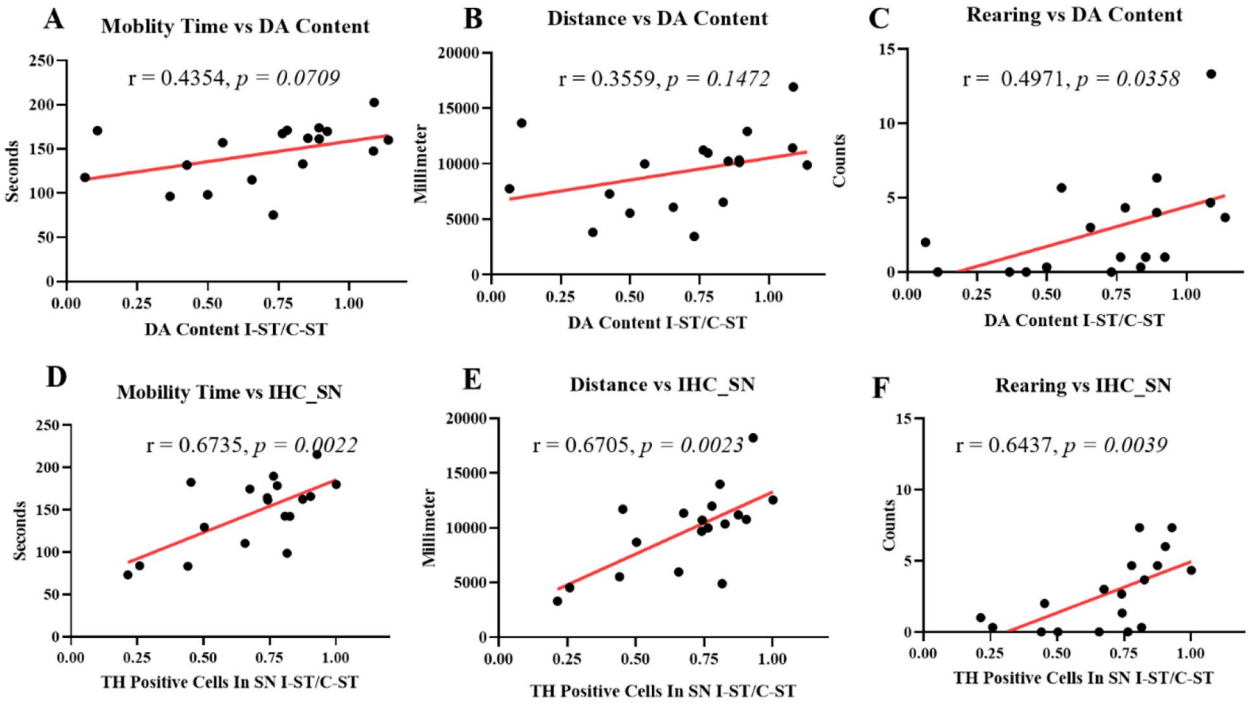

Fig. 7 Correlation Analysis Between Behavioral, Immunohistochemical and Biological Tests
The correlation analysis of the parameters (mobility time, movement distance, and rearing number) from the open field test to the DA content determination (**A**-**C**), and TH positive cells in substantial nigra (**D**-**F**)

16 SD rats and 9 rhesus monkeys (1.75 E-02 mSv/MBq) [55]. The variation in radiation dosimetry estimates between [^{18}F]FECNT-d$_4$ and [^{18}F]FECNT may be attributed to species differences as well as the use of different software (our data implanted in Olinda while these two studies used MIRDOSE 3.1 software). The liver absorbed the highest radioactivity of [^{18}F]FECNT-d$_4$ at 8.73E-03 mSv/MBq. Based on [^{18}F]FDG dosage administration, an examination with 370 MBq of [^{18}F]FECNT-d$_4$ would result in an effective dose of about 1.8 mSv. The radiation dosimetry estimate of [^{18}F]FECNT-d$_4$ compares favorably with the non-deuterium [^{18}F]FECNT and falls within the same range as [^{99m}Tc]TRODAT-1, another DAT imaging agent [56]. These findings suggest that [^{18}F]FECNT-d$_4$ may be a safe and effective radiotracer for the visualization of DAT and has promising potential for successful clinical translation.

Conclusion

This study suggests that PET scanning with [^{18}F]FECNT-d$_4$ could aid in grading and diagnosing Parkinson's disease in its early stages by distinguishing different degrees of dopaminergic denervation in the nigrostriatal system in rats. Quantitative PET imaging correlated well with behavioral, biochemical, and immunohistochemical tests. In vitro autoradiography confirmed [^{18}F]FECNT-d$_4$'s ability to detect dopamine neuron density in human PD and control striatal sections. Radiation dosimetry extrapolation suggests [^{18}F]FECNT-d$_4$ is clinically safe. All these results indicated its potential as a PET radioligand for clinical use in diagnosing Parkinson's disease, even in its early stages. In summary, [^{18}F]FECNT-d$_4$ shows promise for visualizing DAT degeneration in Parkinson's disease and warrants further clinical evaluation.

Abbreviations

PD	Parkinson's Disease
PET	Positron Emission Tomography
[^{18}F]FECNT	2β-Carbomethoxy-3β-(4-chlorophenyl)-8-(2-[^{18}F]-fluoroethyl) nortropane
[^{18}F]FECNT-d$_4$	2β-Carbomethoxy-3β-(4-chlorophenyl)-8-(2-[^{18}F]-fluoroethyl-1,1,2,2-d$_4$) nortropane
6-OHDA	6-Hydroxydopamine Hydrochloride
SUV	Standardized Uptake Value
[^{18}F]F-DOPA	L-3,4-dihydroxy-6-^{18}Ffluoro-phenyl-alanine
AADC	L-amino acid decarboxylase
VMAT2	Vesicular Monoamine Transporter
DAT	Dopamine Transporter
DA	Dopamine
APO	Apomorphine
MsOECNT-d$_4$	2β-Carbomethoxy-3β-(4-Chlorophenyl)-8-(2-((methylsulfonyl)-oxy) ethyl-1,1,2,2-d$_4$)-nortropane
ROI	Region of Interest
ST	Striatum
CB	Cerebellum
SUV	Standardized Uptake Value
SUVr	Standardized Uptake Value Ratio
OFT	Open Field Test
PBS	Phosphate-buffered Saline
O.C.T.	Optimal Cutting Temperature

SN	Substantia Nigra
DAB	3,3′-Diaminobenzidine Tetrahydrochloride
TH	Tyrosine Hydroxylase
IOD	Integral Optical Density
I-ST	Ipsilateral Striatum
C-ST	Contralateral Striatum
I-SN	Ipsilateral Substantia Nigra
C-SN	Contralateral Substantia Nigra
HPLC	High-Performance Liquid Chromatography
ECD	Electrochemical Detection
DOPAC	3,4-Dihydroxyphenylacetic Acid
HVA	Homovanillic Acid
EDTA	Ethylenediaminetetraacetic Acid
ARG	Autoradiography
DLU	Digital Light Units
SEM	Standard Error of The Mean
SD	Standard Deviation
ANOVA	One-Way Analysis of Variance
IHC	Immunohistochemical
BBB	Blood-Brain Barrier
C-H	Carbon-Hydrogen
C-D	Carbon-Deuterium
[^{18}F]FP-CIT	[^{18}F]N-3-Fluoropropyl-2β-carbomethoxy-3β-(4-iodophenyl) nortropane
SD	Sprague-Dawley

Acknowledgements
Not applicable.

Authors' contributions
JT participated in all procedures of this study and was a major contributor to writing the manuscript. CjL analyzed and interpreted radiation dosimetry data. CyL, QyH, and YF made indispensable contributions to chemical and radiochemical synthesis. ZpC provided instructive advice on experimental design and manuscript writing. All authors read and approved the final manuscript.

Funding
The present work was supported by the National Natural Science of China (82172054), the Natural Science of Jiangsu Province (BK20210062), Science and Technology Project of Wuxi Administration of Traditional Chinese Medicine (ZYKJ202115). Science and Technology Project of Jiangsu Administration of Traditional Chinese Medicine (MS2022144).

Data availability
The datasets used and/or analyzed during the current study are available from the corresponding author upon reasonable request.

Declarations

Ethics approval and consent to participate
All animal experiments were approved by the Animal Care and Use Committee of Jiangsu Institute of Nuclear Medicine and conducted in compliance with institutional guidelines (Approved number: JSINM-2023-061). Postmortem human brain tissues from control and PD patient subjects were obtained from the Chinese Brain Bank Center, with experiments approved by the Ethics, Science and Technology Committee of Central South University (Committee's reference number: 2022-scuec-039). The use of human postmortem brain tissues was also approved by the ethics committee of our institute (Approved number: YLK-202329), and all procedures were in accordance with ethical standards. The study was carried out in compliance with the ARRIVE guidelines, and all methods adhered to relevant guidelines and regulations.

Chemicals
All reagents and solvents used in the study were purchased from reputable suppliers such as Sigma-Aldrich, Cayman Chemistry Company (USA), ABX (Germany), J&K Scientific (China), or Aladdin (China) and were used without further purification. Sep-Pak C18 cartridge and Sep-Pak Light QMA used during radiosynthesis were obtained from Waters (Milford, MA, USA).

Biological
Male Sprague-Dawley (SD) rats weighing 250–300 g were purchased from Cavens Laboratory Animal Co., Ltd. (Jiangsu, China), and were housed following the Chinese Guidelines for Animal Research. Postmortem human brain tissues from control and PD patient subjects were obtained from the Chinese Brain Bank Center. Mouse anti-tyrosine hydroxylase (TH antibody) was a commercial product of Sigma Corporation with the code T2928.

Consent for publication
Not applicable.

Competing interests
The authors declare that they have no competing interests.

Conflict of interest
The authors declare that they have no conflict of interest.

Author details
[1]NHC Key Laboratory of Nuclear Medicine, Jiangsu Key Laboratory of Molecular Nuclear Medicine, Jiangsu Institute of Nuclear Medicine, No. 20 Qianrong Road, Binhu District, Wuxi 214063, China
[2]Department of Nuclear Medicine, Huashan Hospital, Fudan University, No. 12 Wulumuqi Middle Road, Jing'an District, Shanghai 200040, China

Received: 13 April 2024 / Accepted: 16 August 2024
Published online: 29 August 2024

References

1. Zheng Z, Zhu Z, Zhou C, Cao L, Zhao G. Burden of Parkinson Disease in China, 1990–2019: findings from the 2019 global burden of Disease Study. Neuroepidemiology. 2023;57:51–63. https://doi.org/10.1159/000527372
2. Feigin VL, Nichols E, Alam T, Bannick MS, Beghi E, Blake N, et al. Global, regional, and national burden of neurological disorders, 1990–2016: a systematic analysis for the global burden of Disease Study 2016. Lancet Neurol. 2019;18:459–80. https://doi.org/10.1016/s1474-4422(18)30499-x
3. Armstrong MJ, Okun MS. Diagnosis and treatment of Parkinson Disease. JAMA. 2020;323:548–60. https://doi.org/10.1001/jama.2019.22360
4. Tolosa E, Garrido A, Scholz SW, Poewe W. Challenges in the diagnosis of Parkinson's disease. Lancet Neurol. 2021;20. https://doi.org/10.1016/s1474-4422(21)00030-2. :385 – 97.
5. Bidesi NSR, Vang Andersen I, Windhorst AD, Shalgunov V, Herth MM. The role of neuroimaging in Parkinson's disease. J Neurochem. 2021;159:660–89. https://doi.org/10.1111/jnc.15516
6. Politis M. Neuroimaging in Parkinson disease: from research setting to clinical practice. Nat Rev Neurol. 2014;10:708–22. https://doi.org/10.1038/nrneurol.2014.205
7. Gee AD, Herth MM, James ML, Korde A, Scott PJH, Vasdev N. Radionuclide Imaging for Neuroscience: current opinion and future directions. Mol Imaging. 2020;19:1–9. https://doi.org/10.1177/1536012120936397
8. Lameka K, Farwell MD, Ichise M. Positron Emission Tomography. Handb Clin Neurol. 2016;135:209–27. https://doi.org/10.1016/B978-0-444-53485-9.00011-8
9. Saeed U, Compagnone J, Aviv RI, Strafella AP, Black SE, Lang AE, et al. Imaging biomarkers in Parkinson's disease and parkinsonian syndromes: current and emerging concepts. Transl Neurodegener. 2017;6:25. https://doi.org/10.1186/s40035-017-0076-6
10. Lotankar S, Prabhavalkar KS, Bhatt LK. Biomarkers for Parkinson's Disease: recent Advancement. Neurosci Bull. 2017;33:585–97. https://doi.org/10.1007/s12264-017-0183-5
11. Stoessl AJ. Positron emission tomography in premotor Parkinson's disease. Parkinsonism Relat Disord. 2007;13:S421–4. https://doi.org/10.1016/s1353-8020(08)70041-5
12. Lee CS, Samii A, Sossi V, Ruth TJ, Schulzer M, Holden JE, et al. In vivo positron emission tomographic evidence for compensatory changes in presynaptic dopaminergic nerve terminals in Parkinson's disease. Ann Neurol. 2000;47:493–503. https://doi.org/10.1002/1531-8249(200004)47:4%3C493::Aid-ana13%3E3.0.Co;2-4
13. Li T, Le W. Biomarkers for Parkinson's Disease: how good are they? Neurosci Bull. 2019;36:183–94. https://doi.org/10.1007/s12264-019-00433-1

14. Mitchell T, Lehéricy S, Chiu SY, Strafella AP, Stoessl AJ, Vaillancourt DE. Emerging neuroimaging biomarkers across Disease Stage in Parkinson Disease. JAMA Neurol. 2021;78:1262–72. https://doi.org/10.1001/jamaneurol.2021.1312
15. Savchenko A, Targa G, Fesenko Z, Leo D, Gainetdinov RR, Sukhanov I. Dopamine transporter deficient rodents: perspectives and limitations for Neuroscience. Biomolecules. 2023;13:20. https://doi.org/10.3390/biom13050806
16. Ng J, Barral S, Waddington SN, Kurian MA. Dopamine Transporter Deficiency Syndrome (DTDS): expanding the clinical phenotype and Precision Medicine approaches. Cells. 2023;12:1737. https://doi.org/10.3390/cells12131737
17. Brucke T, Brucke C. Dopamine transporter (DAT) imaging in Parkinson's disease and related disorders. J Neural Transm (Vienna). 2022;129:581–94. https://doi.org/10.1007/s00702-021-02452-7
18. Mackie P, Lebowitz J, Saadatpour L, Nickoloff E, Gaskill P, Khoshbouei H. The dopamine transporter: an unrecognized nexus for dysfunctional peripheral immunity and signaling in Parkinson's Disease. Brain Behav Immun. 2018;70:21–35. https://doi.org/10.1016/j.bbi.2018.03.020
19. Meles SK, Oertel WH, Leenders KL. Circuit imaging biomarkers in preclinical and prodromal Parkinson's disease. Mol Med. 2021;27:111. https://doi.org/10.1186/s10020-021-00327-x
20. Miller DB, O'Callaghan JP. Biomarkers of Parkinson's disease: present and future. Metabolism. 2015;64:S40–6. https://doi.org/10.1016/j.metabol.2014.10.030
21. Xu J, Xu Q, Liu S, Li L, Li L, Yen T-C, et al. Computer-aided classification Framework of Parkinsonian disorders using ^{11}C-CFT PET imaging. Front Aging Neurosci. 2022;13. https://doi.org/10.3389/fnagi.2021.792951
22. Dean F, Wong B, Yung RF, Dannals EK, Shaya, Hayden T, Ravert CA, Chen B, Chan T, Folio U, Scheffel GA, Ricaurte JL, Neumeyer HN, Wagner JR, AND, Michael J. Kuhar. In Vivo Imaging of Baboon and Human Dopamine Transporters by Positron Emission Tomography Using [^{11}C]WIN 35,428. Synapse. 1993;15:130 – 42. https://doi.org/10.1002/syn.890150205
23. Park HS, Song YS, Moon BS, Yoo SE, Lee JM, Chung YT, et al. Neurorestorative effects of a Novel Fas-Associated factor 1 inhibitor in the MPTP Model: an [^{18}F]FE-PE2I Positron Emission Tomography Analysis Study. Front Pharmacol. 2020;11. https://doi.org/10.3389/fphar.2020.00953
24. Serriere S, Tauber C, Vercouillie J, Guilloteau D, Deloye JB, Garreau L, et al. In vivo PET quantification of the dopamine transporter in rat brain with [^{18}F]LBT-999. Nucl Med Biol. 2014;41:106–13. https://doi.org/10.1016/j.nucmedbio.2013.09.007
25. Cheon M, Kim SM, Ha S-W, Kang MJ, Yang H-E, Yoo J. Diagnostic performance for Differential diagnosis of atypical parkinsonian syndromes from Parkinson's Disease using quantitative indices of ^{18}F-FP-CIT PET/CT. Diagnostics. 2022;12:1402. https://doi.org/10.3390/diagnostics12061402
26. Palermo G, Ceravolo R. Molecular imaging of the dopamine transporter. Cells. 2019;8:872. https://doi.org/10.3390/cells8080872
27. Masilamoni G, Votaw J, Howell L, Villalba RM, Goodman M, Voll RJ, et al. ^{18}F-FECNT: validation as PET dopamine transporter ligand in parkinsonism. Exp Neurol. 2010;226:265–73. https://doi.org/10.1016/j.expneurol.2010.08.024
28. Margaret R, Davis JRV, Douglas Bremner J, Byas-Smith MG, Faber TL, Voll RJ, Hoffman JM, Scott T, Grafton CD, Kilts. Goodman. Initial Human PET Imaging Studies with the dopamine transporter ligand ^{18}F-FECNT. J Nucl Med. 2003;44:855–61. https://jnm.snmjournals.org/content/44/6/855.long
29. Sami S, Zoghbi H, Umesha Shetty M, Ichise M, Fujita M, Imaizumi J-S, Liow J, Shah JL, Musachio, Victor W, Pike. Innis. PET imaging of the dopamine transporter with ^{18}F-FECNT: a Polar Radiometabolite confounds Brain Radioligand measurements. J Nucl Med. 2006;47:520–7. https://jnm.snmjournals.org/content/47/3/520.long
30. Kuchar M, Mamat C. Methods to increase the Metabolic Stability of ^{18}F-Radiotracers. Molecules. 2015;20:16186–220. https://doi.org/10.3390/molecules200916186
31. Timmins GS. Deuterated drugs: where are we now? Expert Opin Ther Pat. 2014;24:1067–75. https://doi.org/10.1517/13543776.2014.943184
32. Guengerich FP. Kinetic deuterium isotope effects in Cytochrome P450 reactions. Methods Enzymol. 2017;596:217–38. https://doi.org/10.1016/bs.mie.2017.06.036
33. Zhao R, Zha Z, Yao X, Ploessl K, Choi SR, Liu F, et al. VMAT2 imaging agent, D6-[^{18}F]FP-(+)-DTBZ: improved radiosynthesis, purification by solid-phase extraction and characterization. Nucl Med Biol. 2019;72–73:26–35. https://doi.org/10.1016/j.nucmedbio.2019.07.002
34. Joanna S, Fowler G-JW, Logan J, Xie S, Volkow ND, Robert R, MacGregor, DJ, Schlyer NP, Alexoff DL. Clifford Patlak and Alfred P. Wolf. Selective Reduction of Radiotracer Trapping by Deuterium Substitution Comparison of Carbon4l-L-Deprenyl and Carbon-11-Deprenyl-D2 for MAO B Mapping. J Nucl Med. 1995;36:1255-62. https://jnm.snmjournals.org/content/36/7/1255.long.
35. Nag S, Jahan M, Toth M, Nakao R, Varrone A, Halldin C. PET imaging of VMAT2 with the Novel Radioligand [^{18}F]FE-DTBZ-d4 in Nonhuman Primates: comparison with [^{11}C]DTBZ and [^{18}F]FE-DTBZ. ACS Chem Neurosci. 2021;12:4580–6. https://doi.org/10.1021/acschemneuro.1c00651
36. Graham Smith Y, Zhao J, Leyton B, Shan Quang-de, Nguyen M, Perumal D, Turton E, Årstad SK, Luthra EG, Robins, Eric O. Aboagye. Radiosynthesis and pre-clinical evaluation of [^{18}F]fluoro-[1,2-^{2}H$_4$]choline. Nucl Med Biol. 2011;38:39–51. https://doi.org/10.1016/j.nucmedbio.2010.06.012
37. Cao S, Tang J, Liu C, Fang Y, Ji L, Xu Y, et al. Synthesis and biological evaluation of [^{18}F]FECNT-d$_4$ as a Novel PET Agent for dopamine transporter imaging. Mol Imaging Biol. 2021;23:733–44. https://doi.org/10.1007/s11307-021-01603-2
38. Tang J, Xu Y, Liu C, Fang Y, Cao S, Zhao C, et al. PET imaging with [^{18}F]FP-(+)-DTBZ in 6-OHDA-induced partial and full unilaterally-lesioned model rats of Parkinson's disease and the correlations to the biological data. Nucl Med Biol. 2020;90–91:1–9. https://doi.org/10.1016/j.nucmedbio.2020.08.002
39. Xu Y, Tang J, Liu C, Zhao C, Cao S, Yu H, et al. MicroPET imaging of vesicular monoamine transporter 2 revealed the potentiation of (+)-dihydrotetrabenazine on MPTP-induced degeneration of dopaminergic neurons. Nucl Med Biol. 2021;96–97:9–18. https://doi.org/10.1016/j.nucmedbio.2021.02.004
40. Liu C, Tang J, Xu Y, Cao S, Fang Y, Zhao C, et al. Molar activity of [^{18}F]FP-(+)-DTBZ radiopharmaceutical: determination and its effect on quantitative analysis of VMAT2 autoradiography. J Pharmaceut Biomed. 2021;203:114212. https://doi.org/10.1016/j.jpba.2021.114212
41. Chang CH, Chang YJ, Lee TW, Ting G, Chang KP. Dosimetric evaluation of nanotargeted ^{188}Re-liposome with the MIRDOSE3 and OLINDA/EXM programs. Ann Nucl Med. 2012;26:419–25. https://doi.org/10.1007/s12149-012-0593-4
42. Federal Register, Rules. and Regulations; 2018. p. 83416–32.
43. Forsback S, Niemi R, Marjamaki P, Eskola O, Bergman J, Gronroos T, et al. Uptake of 6-[18F]fluoro-L-dopa and [18F]CFT reflect nigral neuronal loss in a rat model of Parkinson's disease. Synapse. 2004;51:119–27. https://doi.org/10.1002/syn.10293
44. Yee RE, Irwin I, Milonas C, Stout DB, Huang SC, Shoghi-Jadid K, et al. Novel observations with FDOPA-PET imaging after early nigrostriatal damage. Mov Disord. 2001;16:838–48. https://doi.org/10.1002/mds.1168
45. Jan Booij GT, Ania Winogrodzka EA, van Royen. Imaging of the dopaminergic neurotransmission system using single-photon emission tomography and positron emission tomography in patients with parkinsonism. Eur J Nucl Med. 1999;26:171–82. https://doi.org/10.1007/s002590050374
46. Blesa J, Pifl C, Sanchez-Gonzalez MA, Juri C, Garcia-Cabezas MA, Adanez R, et al. The nigrostriatal system in the presymptomatic and symptomatic stages in the MPTP monkey model: a PET, histological and biochemical study. Neurobiol Dis. 2012;48:79–91. https://doi.org/10.1016/j.nbd.2012.05.018
47. Choi JY, Kim CH, Jeon TJ, Cho WG, Lee JS, Lee SJ, et al. Evaluation of dopamine transporters and D2 receptors in hemiparkinsonian rat brains in vivo using consecutive PET scans of [18F]FPCIT and [18F]fallypride. Appl Radiat Isot. 2012;70:2689–94. https://doi.org/10.1016/j.apradiso.2012.08.005
48. Hu Q, Li Q, Tang J, Liu J, Fang Y, Liu C, et al. Synthesis and biological evaluation of 18F-labelled deuterated tropane derivatives as dopamine transporter probes. Arab J Chem. 2023. https://doi.org/10.1016/j.arabjc.2023.105278. 16.
49. Shin KH, Park SA, Kim SY, Lee SJ, Oh SJ, Kim JS. Effect of Animal Condition and Fluvoxamine on the result of [(18)F]N-3-Fluoropropyl-2beta-carbomethoxy-3beta-(4-iodophenyl) nortropane ([(18)F]FP-CIT) PET study in mice. Nucl Med Mol Imaging. 2012;46:27–33. https://doi.org/10.1007/s13139-011-0117-5
50. Schoemaker H, Arbilla CPS, Scatton B, Javoy-Agid F, Langer SZ. Sodium dependent [^{3}H]cocaine binding associated with dopamine uptake sites in the rat striatum and human putamen decrease after dopaminergic denervation and in parkinsons disease. N-S Arch Pharmacol. 1985;329:227–35. https://doi.org/10.1007/bf00501873
51. Przedborski S, JIANG MLH, M. Ferreira. Jackson-Lewis,Donaldson and, Togasaki DM. Dose-dependent lesions of the dopaminergic nigrostriatal pathway induced by intrastriatal injection of 6-hydroxydopamine. Neuroscience. 1995;67:631 – 47. https://doi.org/10.1016/0306-4522(95)00066-r
52. Strome EM, Cepeda IL, Sossi V, Doudet DJ. Evaluation of the Integrity of the dopamine system in a Rodent Model of Parkinson's Disease: small animal Positron Emission Tomography compared to behavioral Assessment and Autoradiography. Mol Imaging Biol. 2006;8:292–9. https://doi.org/10.1007/s11307-006-0051-6

53. Chen Z, Tang J, Liu C, Li X, Huang H, Xu X, et al. Effects of anesthetics on vesicular monoamine transporter type 2 binding to ^{18}F-FP-(+)-DTBZ: a biodistribution study in rat brain. Nucl Med Biol. 2016;43:124–9. https://doi.org/10.1016/j.nucmedbio.2015.09.009
54. Dnyanesh N, Tipre MF, Frederick T, Chin N, Seneca D, Vines J-S, Liow VW, Pike, Robert B, Innis. Whole-body biodistribution and radiation dosimetry estimates for the PET dopamine transporter probe ^{18}F-FECNT in nonhuman primates. Nucl Med Commun. 2004;25:737–42. https://doi.org/10.1097/01.mnm.0000133074.64669.60
55. Chen H, Jiang Z, Cheng X, Zheng W, Sun Y, Yu Z, et al. [^{18}F]BIBD-239: ^{18}F-Labeled ER176, a Positron Emission Tomography Tracer Specific for the translocator protein. Mol Pharm. 2022;19:2351–66. https://doi.org/10.1021/acs.molpharmaceut.2c00157
56. Mozley PD, Karl Plossl,Stefan JBS, Dresel H, Barraclough ED, Alavi A, Araujo LI, Hank F. Kung. Biodistribution and Dosimetry of TRODAT-1: a Technetium-99m tropane for imaging dopamine transporters. J Nucl Med. 1998;39:2069–76. https://jnm.snmjournals.org/content/39/12/2069.long

Publisher's note